

Flow and particle deposition simulations with heat-transfer in the nine-generation lung airways

B. Soni, N. Arra, and S. Aliabadi

Northrop Grumman Center for High Performance Computing, Jackson State University, Jackson, MS, USA

Abstract - *The flow fields in lower lung airways are rich in secondary flows in form of vortices. These vortices are known to impact the micro-particle transport in lung airways. The complex geometry of lung airways plays a significant role on the secondary flows generation. Inhaled air temperature may also have an impact on the bronchial tube flows and therefore to the particle deposition. The steady-state inspiratory air flow with and without heat-transfer were simulated in a nine-generation lung airway model using our in-house flow-solver. Particle traces were simulated using our Lagrangian based particle tracking software. The flow and particle trace simulation results with and without heat-transfer were compared. The effects of heat-transfer on the flow fields and particle deposition in the lung model were found to be insignificant suggesting that, the thermal effects can be overlooked when simulating the flow and particle transport in the small lung airways.*

Keywords: *biomechanics, lung airways, particle deposition, lung flow, computational Fluid Dynamics (CFD)*

1 Introduction

The complexity of lung air flow fields exists mainly due to the presence of secondary flows in form of vortices. These vortices are generated as a result of the bifurcating geometry of the bronchial tubes. The secondary flows are known to play a crucial role in particle transport from inhaled air. The study of bronchial tube flows can increase an understanding of the effects of the inhalation of harmful particles as well as the pulmonary drug delivery to improve human health. Particles suspended in the atmosphere are of various sizes and shapes [1]. Most of the particles from the atmosphere found inside the human lungs range in size from $2\text{-}10\mu\text{m}$, corresponding to coal dust, asbestos fiber, pollen, bacteria, etc [1]. There have been some studies identifying the health risks related to inhalation of micro- or nano-particles[2-9].

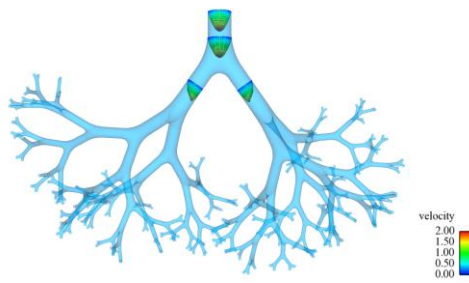
The bronchial tube geometry is characterized by bifurcations that produce multiple generations with asymmetric and nonplanar branching. There are a total of 18 generations (excluding the alveolus) [10] of airways in the human airway tree that consists of 2^{17} distinct tubes. The out-of-plane branch angles defining nonplanarity are randomly distributed to fill the chest cavity without any overlap. The effects of nonplanarity for asymmetric three-generation bronchial tube flow fields were investigated for three-

generation bronchial tube models by Soni et al. [11]. They also demonstrated significant difference between the particle deposition in the planar and nonplanar three-generation bronchial tube models [12].

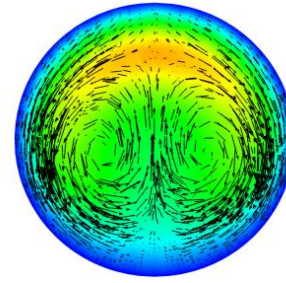
The flows in small bronchial tubes are laminar with a Reynolds number less than 1000 [13]. However, the presence of vortices makes these flows quite complicated. The effects of secondary flow on particle dispersion were demonstrated by Soni et al. [12]. They used particle destination and Finite Time Lyapunov (FTLE) maps [14] to visualize particle deposition. The flow becomes more complex further down the tree due to the accumulative effects of nonplanarity and multiple generations. The bronchial tube flows can be categorized as primary and secondary flows. The flow in the direction of the local axis of the tube is called primary flow. The flows perpendicular to the local axis of the tube are called secondary flows. Figure 1 demonstrates the primary and secondary flows in the bronchial tubes. Figure 1(a) shows the primary velocity vectors at various cross-sections in the nine-generation bronchial tube model. The vectors are colored by dimensionless velocity magnitude. The secondary flows in form of a vortex pair in the second generation are shown in Figure 1(b). The cross-flow velocity vectors are plotted on the cutting plane which is colored by total velocity magnitude.

There have been some studies to simulate flows in bronchial tubes with more than just few generations in effort to achieve flow simulation of fully resolved bronchial tree. Nowak et al. [15] presented flow fields and particle transport simulations on lung airways with multigenerational symmetric planar model for up to 23 generations and a CT-scan model with nine generations. Ertbruggen et al. [16] described a lung airway model with eight generations containing 17 bifurcations and simulated steady-state flow with micro-particle transport. Gemci et al. [17] presented a simulation of 17 generations of the human lung based on the anatomical model of Schmidt et al. [18]. The geometry was only partially resolved, containing only 1453 bronchi as opposed to 2^{17} branches. In more recent efforts, Walters and Luke [19] proposed a Flow Path Ensemble (FPE) model to simulate flows in a nine-generation model with the model truncated so that the overall size of simulation was significantly reduced.

Thermal effects of the inhaled air temperature on the flow fields and particle deposition may become important when cold air or hot vapor is being inhaled. There are few experimental and numerical studies addressing heat-transfer in the lung airways [20-23]. The heat-transfer and mass-transfer was simulated for hot vapor by Zhang et al. [22]. They also



a) Primary velocities in first bifurcation



b) Secondary velocities at cross-section in second generation tube

Figure 1. Bronchial tube flow fields.

studied the effect of cold weather on the steady state flow fields and particle deposition. The impact of temperature difference was found to be pronounced in the mouth to trachea geometry, whereas the thermal effects were found to be deteriorating in downstream generations. The effects were evaluated for three-generation, symmetric, planar bronchial tube model along with airway from mouth to trachea. In later study [23], they investigated heat-transfer and mass-transfer for hygroscopic droplets with unsteady flow conditions in same lung airway model.

2 Numerical modeling

The nine-generation geometry as shown in Figure 1(a), given by Walters and Luke [19], based on Weibel's [24] morphology for generations 4-12 of the human bronchial tree was employed in this study. A single parent tube being one-generation, two daughter tubes diverging from a parent tube defines two generations. A general expression to obtain total number of exits based on number of generations can be given as $N_{exit} = 2^{N-1}$, where N is the number of generations and N_{exit} is the number of exits. The parent tube diameter was taken to be $0.0057m$. The out-of-plane angles defining nonplanarity are randomly distributed between 0° to 180° . There are in total $2^8 = 256$ exits in this model.

Steady-state inhalation with Reynolds number of 319 corresponding to an inlet volumetric flow rate of $20.83 \text{ cm}^3/s$ were simulated with and without heat-transfer. The air flows were simulated by using the CaMEL flow solver.²⁵ CaMEL is an advanced computational fluid dynamics flow solver specifically developed for large scale simulations at the Northrop Grumman Center for High Performance Computing at Jackson State University. CaMEL is a highly scalable, incompressible, non-dimensional code. CaMEL is a hybrid finite volume/element solver, which takes advantage of the merits of both the Finite Volume and Finite Element methods and avoids their shortcomings. The buoyancy force was included in the momentum equation to capture the thermal effects while simulating the heat-transfer in the nine-generation model. A Grashof number of 1388 corresponding to the temperature difference of 47° C was utilized. Grashof number is dimensionless parameter which provides a ratio of buoyancy forces to the viscous forces. The bronchial tube

walls were assumed to be at the normal body temperature (37°C) and inhaled air temperature during cold weather condition (-10°C). At the inlet, a parabolic velocity and uniform temperature profiles were applied. No-slip condition with isothermal temperature was applied on the tube walls. At the exits, zero static pressure was specified. The nondimensional temperature is given by $T^* = (T - T_{wall}) / (T_{in} - T_{wall})$, where T is the temperature, T_{in} is the inlet temperature and T_{wall} is the bronchial tube wall temperature. A fully unstructured mesh was employed for discretization of the nine-generation bronchial tube model. The commercial software package Gridgen [26] was utilized to generate high quality mesh. The final mesh consisted of approximately 40 million tetrahedral elements.

The particle traces were simulated as a post-processing step using a Lagrangian method. Water droplets with a diameter of $10\mu\text{m}$ were released from the inlet of the model. Approximately 34000 particles were released at the inlet. The particles were released from the nodes of the uniform triangular mesh at the inlet. The initial velocities of the particles were kept the same as the inlet fluid velocities. Since impaction plays an important role for micro-particle transport, drag and gravitational forces were included in the equation of motion. The fourth-order Runge-Kutta method was used to integrate the equation of motion.

3 Results

The results of the flow fields and particle trajectory simulations for the nine-generation bronchial tube model with and without heat-transfer are shown and compared in this section. The comparison of the various metrics is made to investigate the thermal impact on the flow fields and particle deposition. The localized flows in second-generation in terms of primary and secondary velocities are shown in figure 1. A symmetric vortex pattern is observed in figure 1(b) due to the fact that the second-generation is symmetric with respect to the bifurcation plane. Figure 2 shows the primary and secondary velocities in the third-generation branching. In figure 2 (b) asymmetric pattern of vortices are observed since the third-generation branching is locally nonplanar. Now we focus on one of the eighth-generation branches. Primary and secondary flows are shown at a cross-section of one of the

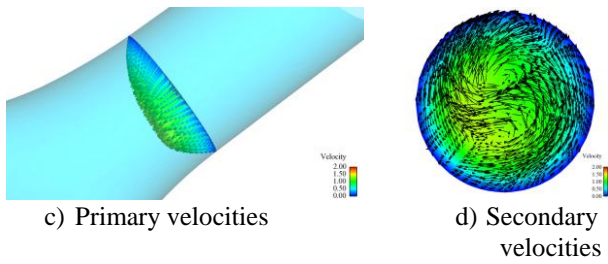


Figure 2. Flows in third-generation.

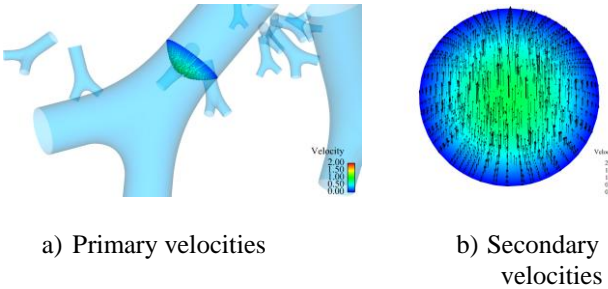


Figure 3. Flows in eighth-generation.

branches of the eighth-generation in figure 3. It can be observed here that, the secondary flows are not dominated by the vortices as the flow rate is not large enough to generate vortices.

In figure 4, dimensionless temperature variation at the cutting plane located in the first bifurcation is shown. The temperature profiles are also shown at various cross-sections perpendicular to the local axis of the tubes. Here, the dimensionless inlet temperature is one and at the bronchial tube walls it is zero. The temperature profiles are skewed towards the center of the bifurcation similar to the velocity profiles. This is because high velocity fluid carries the inlet temperature towards the center of the bronchial tubes.

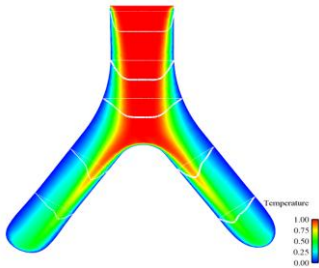


Figure 4. Temperature distribution in first bifurcation

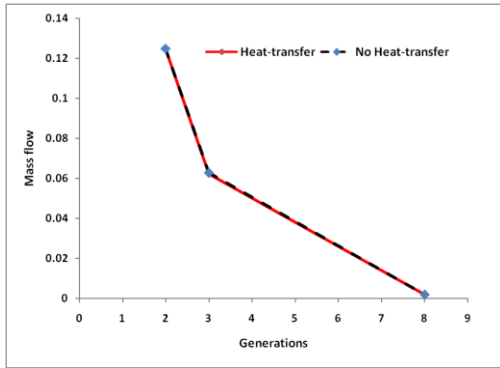
Now to investigate the impact of heat-transfer on the bronchial tube flows, mass flow rate and secondary flow intensity comparisons are made as shown in Figure 5. Results are extracted at cross-sections located in generation-2, generation-3, and generation-8. As the number of generations increases, the tube diameter decreases and therefore the mass flow entering each branch also decreases as observed in Figure 5(a). The secondary velocities at these cross-sections can be quantified by measuring intensity of the secondary flows. The intensity of the secondary flows is defined as the ratio of the averaged local secondary velocities with respect to

the averaged local primary velocity in a given cross-section. The intensities of secondary velocities were also plotted at each cross-section location for both with and without heat-transfer cases. Figure 5(b) shows the variation of the intensity of secondary flows. The values of mass flow and intensity of secondary flows with and without heat-transfer show minimal differences (see figure 5).

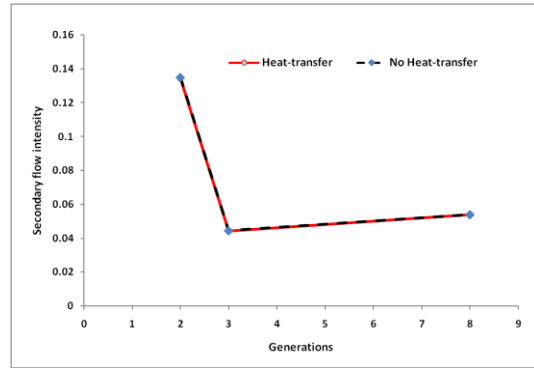
To further assess the effects of heat-transfer, primary velocity profiles were plotted on the line segment passing through the middle of the cross-sections to compare the results for both cases. In Figure 6(a), the comparison between the primary velocities in simulation with and without heat-transfer cases in the second-generation is made. The dimensionless velocities along the length of the line segment are plotted. Similarly, velocity distributions in third- and eighth-generations are shown in figure 6(b) and 6(c), respectively. From figures 6(a)-(c) it can be observed that, the differences between the two velocity profiles for all three plots are insignificant. This suggests negligible thermal effects on local flow fields.

Since flows in the bronchial tube are unaffected by the temperature difference between inlet and tube walls, it can be indirectly implied that the particle deposition will also show minimal sensitivity to the temperature differences. However, we simulate particle trajectories to study particle deposition in order to explicitly investigate the heat-transfer effects on the particle deposition. We compare the particle deposition efficiencies in each generation for the simulation with and without heat-transfer in figure 7. Particle deposition efficiency is defined as the ratio of percent particle deposition to the incoming particles in each generation. As it was predicted, the thermal effects on particle deposition are minimal as the particle deposition efficiencies are quite close to each other for both cases. In general, the particle deposition efficiency increases as we go further down the generations, except in the eight-generation. The reason being, most of the particles entering the eighth generation are exited from the outlets and that result in to the low particle deposition efficiency.

Figure 8 shows particle deposition in nine-generation bronchial tubes in terms of particle destination and FTLE maps. Particle destination map shows the scalar values at particles' release location equal to the generation number it deposited to. Figure 8(a) shows the color map of the generations for particle destination map. Figures 8(b) and 8(c) show the particle destination and FTLE maps, respectively. For example, particles released from the dark blue region of the particle destination map shows that they deposit in the second generation. FTLE map shows the deposition behavior of closely seeded particles inside the generation. Higher FTLE values (red region) implies that the particles released from here are being more dispersed than the particles released at lower FTLE values (blue region). This phenomenon can be explained in detail from figure 9. We release particles from the high FTLE values (purple traces) and low FTLE values (magenta traces) and follow their path and how they are being affected by the geometry and secondary flows of the nine-generation bronchial tube as shown in figure 9(a). The particle

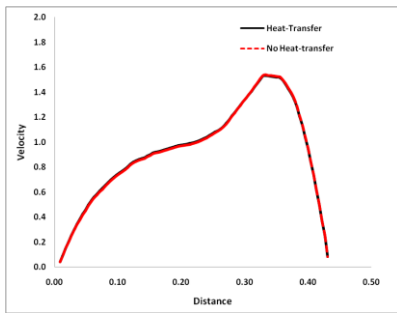


a) Mass flow variation in generations

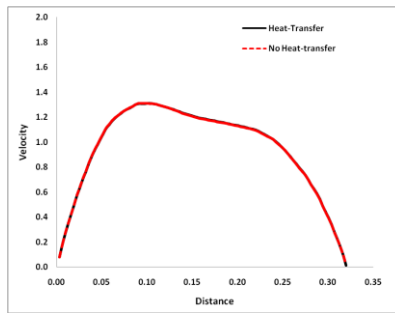


b) Secondary flow intensity variation in generations

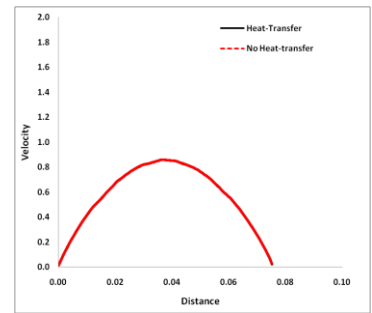
Figure 5. Mass flow and secondary flow intensity comparison.



a) Second-generation



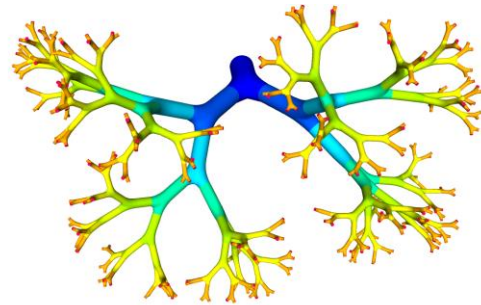
b) Third-generation



c) Eighth-generation

Figure 6. Comparison of dimensionless velocity profiles in generations-2, 3, and 8.

release locations are shown in detail in figure 9(b). In second generation, particles interact with the vortices here as shown in figure 9(c). Since purple particles are passing through the higher cross-flow velocity region, they get more affected by the vortex and get dispersed. Eventually, due to the combined effects of the vortex and geometry they diverge their paths and go to different tube after the first bifurcation. In the third-generation tube, the magenta particle traces are being more affected by one of the vortices and being dispersed (see figure 9(d)). However, the vortex is not strong enough to diverge the



a) Color map for destination map

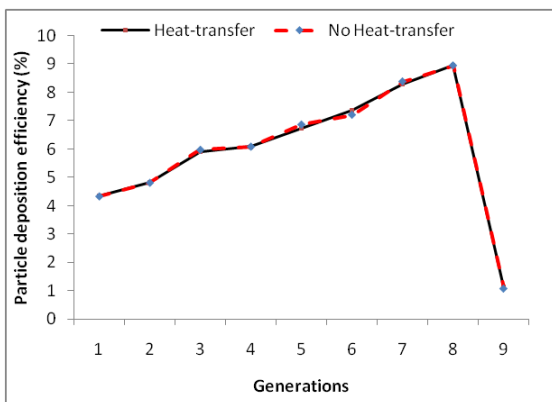
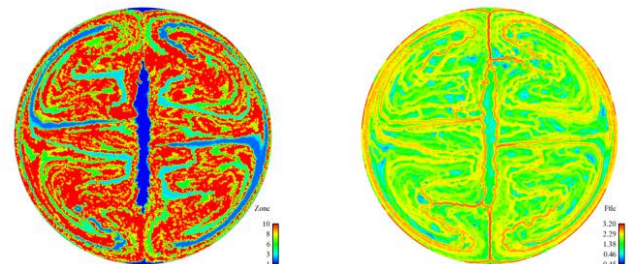
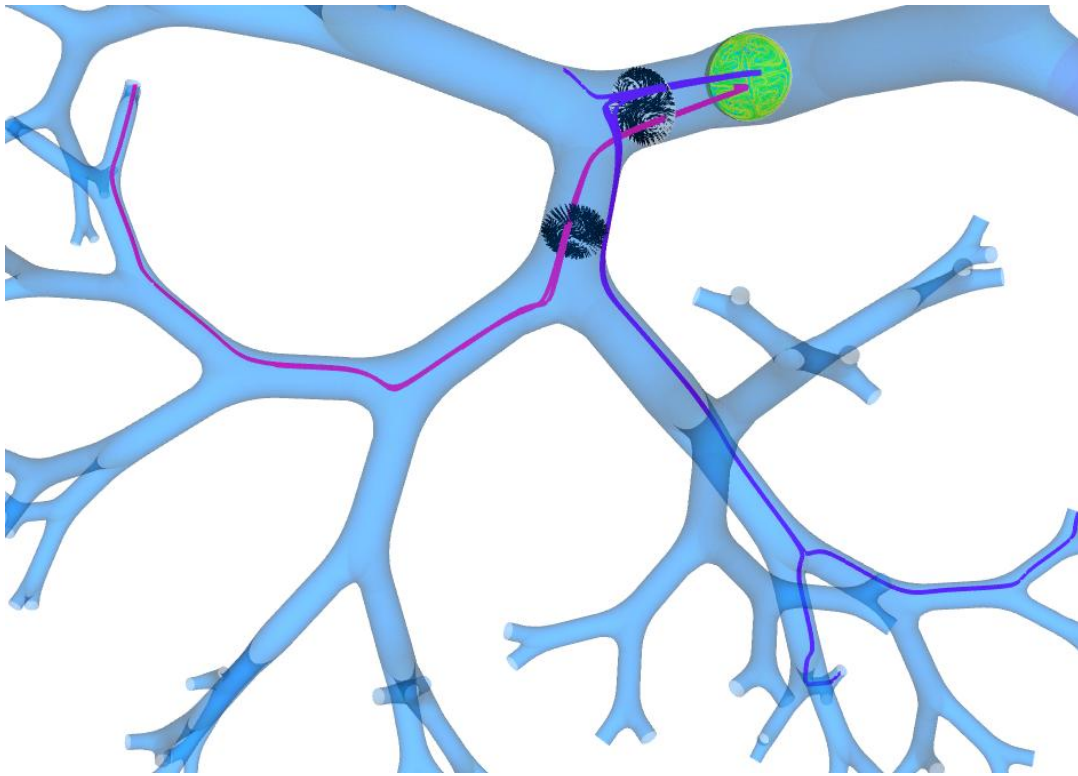


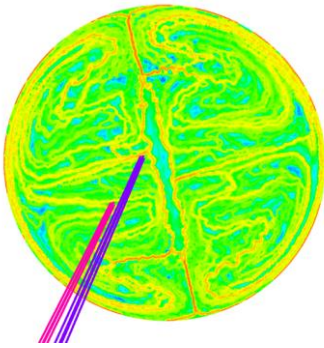
Figure 7. Comparison of particle deposition efficiency in each generation.



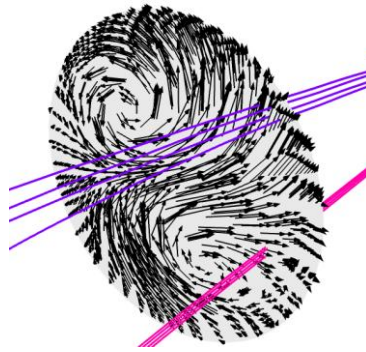
b) Particle destination map c) FTLE map
Figure 8. Particle deposition in bronchial tube model.



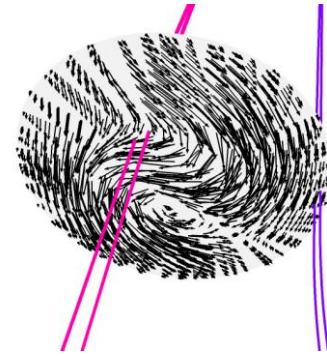
a) Particle traces in nine-generation bronchial tube model



b) FTLE map and particle release location



c) Vortices in the second-generation interacting with particles



d) Vortices in the third-generation interacting with particles

Figure 9. Particle traces in the nine-generation bronchial tube model.

particles' path into different next generation tubes. As a result, they still travel to the same next generation tube. After the third-generation, particles are being more affected by the nonplanar, multigenerational geometry than the vortices as the vortices get weaker with increasing number of generations.

4 Conclusions

Main objective of this paper is to understand and identify the importance of thermal effects of the inhaled air temperature on the flow and particle deposition in the small bronchial tubes. The results suggest that, the effects of the

differences between inhaled air temperature and lung tube wall temperature have little impact on the flow fields and particle deposition in the small bronchial tubes corresponding to the 4-12 generations of lung airway network. Therefore, simulating flow and particle transport with heat-transfer do not appear to be meaningful for the small bronchial tube models, based on this study.

We also try to understand the effects of bronchial tube geometry with multiple bifurcations on the flows and particle deposition. The results showed that particle transport in nine-generation bronchial tubes is mainly driven by the vortices and the nine-generation geometry. It was observed that the impact

of vortices is prominent when particles are in first few generations where the vortices are stronger compared to the ones in further generations. After that, the particle paths are influenced mainly by the nonplanarity of the bronchial tube geometry.

5 Acknowledgments

We would like to thank National Science Foundation (NSF) for funding this research through grant No. EPS-0903787. We would also like to thank Dr. Keith Walters and William Luke for providing us with the geometry of the nine-generation bronchial tube model.

6 References

- [1] American Society of Heating, R. and Engineers, A.-C., *Fundamentals Handbook*, Vol. Chapter 11: Air contaminants, ASHRAE, 1977.
- [2] Higenbottam, T., Siddons, T., and Demoncheaux, E., "The direct and indirect action of inhaled agents on the lung and its circulation: Lessons for clinical science," *Environmental Health Perspectives*, Vol. 109, No. 4, 2001, pp. 559–562.
- [3] Wang, X. and Christiani, D., "Respiratory symptoms and functional status in workers exposed to silica, asbestos, and coal mine dusts," *Journal of Occupational and Environmental Medicine*, Vol. 42, 2000, pp. 1076–1084.
- [4] Inglesby, T., O'Toole, T., and Henderson, D., "Anthrax as a biological weapon, 2002: updated recommendations for management," *Journal of American Medical Association*, Vol. 287, 2002, pp. 2236–2252.
- [5] Lane, H., Montagne, J., and Fauci, A., "Bioterrorism: a clear and present danger," *Nature Medicine*, Vol. 7, 2001, pp. 1271–1273.
- [6] Dockery, D., Pope, C., Xu, X., Spengler, J., Ware, J., Fay, M., Ferris, B., and Speizer, F., "An association between air pollution and mortality in six U.S. cities," *New England Journal of Medicine*, Vol. 329, 1993, pp. 1759–1759.
- [7] Toren, K., Bergdahl, I., Nilsson, T., and Jarvholm, B., "Occupational exposure to particulate air pollution and mortality due to ischaemic heart disease and cerebrovascular disease," *Occupational Environmental Medicine*, Vol. 64, 2007, pp. 515–519.
- [8] Peters, A., Dockery, D., Muller, J., and Mittleman, M., "Increased particulate air pollution and the triggering of myocardial infarction," *Circulation*, Vol. 103, 2001, pp. 2810–2815.
- [9] Pope, C., Muhlestein, J., May, H., Renlund, D., Anderson, J., and Horne, B., "Ischemic heart disease events triggered by short-term exposure to fine particulate air pollution," *Circulation*, Vol. 114, 2006, pp. 2443–2448.
- [10] Warrell, D. A., Cox, T. M., Firth, J. D., and Benz, E. J., *Oxford Textbook of Medicine*, Vol. 2, Oxford University Press, 2003.
- [11] Soni, B., Lindley, C., and Thompson, D., "The Combined Effects of Nonplanarity and Asymmetry on Primary and Secondary Flows in the Small Bronchial Tubes," *International Journal for Numerical Methods in Fluids*, Vol. 59, 2009, pp. 117-146.
- [12] Soni, B., Thompson, D., and Machiraju, R., "Visualizing Particle/Flow Structure Interactions in the Small Bronchial Tubes," *IEEE Transactions on Visualization and Computer Graphics (Proceedings of Visualization/Information Visualization 2008)*, Vol. 14, No. 6, 2008, pp. 1412-1419.
- [13] Gatlin, B., Cuichhi, C., Hammersley, J., Olson, D., R.Reddy, and Burnside, G., "Computation of converging and diverging flow through an asymmetric tubular bifurcation," *ASME FEDSM97*, Vol. 3429, 1997, pp. 1–7.
- [14] Haller, G., "Distinguished material surfaces and coherent structures in threedimensional fluid flows," *Physica D*, Vol. 149, 2001, pp. 248–277.
- [15] Nowak, N., Kadake, P., and Annapragada, A., "Computational fluid dynamics simulation of airflow and aerosol deposition in human lungs," *Annals of Biomedical Engineering*, Vol. 31, 2003, pp. 374–390.
- [16] Ertbruggen, C., Hirsch, C., and Paiva, M., "Anatomically based three-dimensional model of airways to simulate flow and particle transport using computational fluid dynamics," *Journal of Applied Physiology*, Vol. 98, 2004, pp. 970–980.
- [17] Gemci, T., Ponyavin, V., Chen, Y., and Collins, R., "Computational model of airflow in upper 17 generations of human respiratory tract," *Journal of Biomechanics*, Vol. 41, 2008, pp. 2047–2054.
- [18] Schmidt, A., Zidowitz, S., A.Kriete, Denhard, T., Krass, S., and Pietgen, H.-O., "A digital reference model of the human bronchial tree," *Computational Medical Imaging and Graphics*, Vol. 28, 2004, pp. 719–723.
- [19] Walters, K., and Luke, W., "A Method for Three-Dimensional Navier-Stokes Simulations of Large-Scale Regions of the Human Lung Airway", *ASME Journal of Fluids Engineering*, Vol. 132, 2010, Paper No. 051101.

[20] Aref'ev, K., Fedotov, E., and Khrushchenko A., "Nonstationary Heat Exchange in the Trachea of Human Lungs", *Journal of Engineering Physics and Thermophysics*, Vol. 76, No. 4, 2003, pp. 892-898.

[21] Serikov, V., Fleming, N., Talalov, V., and Stawitcke, F., "Effects of the Ventilation Pattern and Pulmonary Blood Flow on Lung Heat Transfer", *European Journal of Applied Physiology*, Vol. 91, 2004, pp. 314-323.

[22] Zhang, Z., and Kleinstreuer, C., "Species Heat and Mass Transfer in a Human Upper Airway Model", *International Journal of Heat and Mass Transfer*, Vol. 46, 2003, pp. 4755-4768.

[23] Zhang, Z., Kleinstreuer, C., and Kim, C., "Water Vapor Transport and its Effects on the Deposition of Hygroscopic Droplets in a Human Upper Airway Model", *Aerosol Science and Technology*, Vol. 40, 2006, pp. 1-16.

[24] Weibel, E., "Morphometry of the human lung," 1963.

[25] Tu, S., and Aliabadi, S., "Development of a hybrid finite volume/element solver for incompressible flows", *International Journal of Numerical Methods in Fluids*. 2007; 55:177-203.

[26] Gridgen, Grid and Mesh generation for Computational Fluid Dynamics (CFD), Software Package, Ver. 15, Fort Worth, TX, 2010.